Two-Stage Correction for Wideband Wireless Signal Generators with Time-Interleaved Digital-to-Analog-Converters

Youngcheol Park[*], *and Kate A. Remley*[**]
[*]*Hankuk Univ. of Foreign Studies, South Korea*
[**]*National Institute of Standards and Technology, Boulder, CO 80305*

Abstract — We present a correction technique for arbitrary waveform generators that utilize time-interleaved digital-to-analog converters. By correcting non-ideal responses of the digital-to-analog converters, the overall signal quality of the source can be improved. To verify this technique, the improvement in a 64-quadrature-amplitude-modulated waveform with a bandwidth of 1.25 GHz was evaluated. The error vector magnitude of the source was improved from 7.8 % to 0.7% with the proposed corrections.

Index Terms — Millimeter-wave wireless communications, modulated signal, signal generator, wireless systems.

I. Introduction

Signal sources are needed to study and implement wireless communications in the millimeter-wave regime. Sources based on arbitrary waveform generators and frequency converters have recently been reported [1],[2]. For signal generation at intermediate frequencies (IFs), high-speed arbitrary waveform generators (AWG) directly generate waveforms by utilizing time-interleaved digital-to-analog converters (DACs) [3]. This time-interleaving technique is adopted to overcome the sampling-rate limitation of the individual DACs [4],[5]. With accurate switching between outputs from the two DACs, the final waveform has a sampling rate equivalent to twice that of the individual sampling rate of each DAC. As illustrated below, the DAC outputs add below the Nyquist rate while cancelling out the image signal above the Nyquist rate.

However, because the bandwidth of signals with millimeter-wave carrier frequencies (roughly 10 % of the carrier frequency) may occupy several gigahertz, obtaining a flat frequency response with the self-calibration processes that are provided by the equipment's manufacturer is very difficult. Additionally, any amplitude or timing imbalance between the DACs associated with time interleaving creates errors both at the in-band and the image-band signals. In particular, the in-band error is critical to the error vector magnitude (EVM) of measured communication signals.

To address these issues, and to create a method to accurately calibrate AWGs that incorporate time interleaving, a two-stage correction process is proposed here. Passing waveforms through a digital de-multiplexer allows us to correct for DAC imbalance. This is followed by a system response correction to account for the nonideal frequency response of the DACs. By applying these corrections in predistortion, the AWG can generate high-quality wideband signals, as intended.

II. Time-Interleaved Signal Generation

The time-interleaving technique is now utilized in state-of-the-art measurement equipment with sampling frequencies higher than 20 Giga-samples-per-second (Gsps) [3]. Figure 1 shows a block diagram of the time-interleaving architecture of these arbitrary waveform generators.

For a transmitted signal $x(t)$ the stored waveform, consisting of L digital samples, is defined as follows:

$$x[m] = x(mT_s) = \sum_{m=1}^{L} \left(x(t)\delta(t - mT_s) \right), \qquad (1)$$

where $x[m]$ is the discrete version of $x(t)$ sampled at a period of T_s. This signal will be uploaded to the AWG. To perform interleaving, $x[m]$ is alternately split into separate paths, one for each DAC. The DACs each have an identical sampling period of $2\,T_s$, creating waveforms $x[2k+1]$ and $x[2k]$, which all have the Nyquist frequency of one half of $x[m]$'s.

Because DACs use a zero-order hold circuit to store and dispense electric charges with a sampling period of T_s, the Fourier transform of the first DAC may be expressed as follows

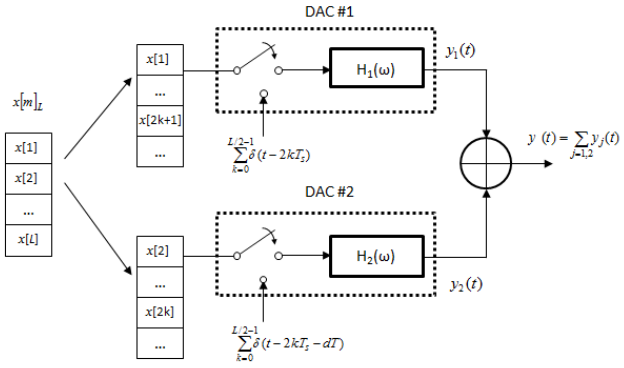

Fig. 1. Operation of time interleaving where the stored $x[m]$ is split and fed into separate DACs, one of which has a timing offset of dT to cancel images at the even-numbered Nyquist zones.

$$Y_1(\omega) = \sum_{n=-\infty}^{\infty} X\left(\omega - \frac{(n-1)\pi}{T_s}\right) H_1(\omega), \quad (2)$$

where $X(\omega)$ is the Fourier transform of the continuous signal $x(t)$ with the angular frequency of ω, and $H_1(\omega)$ is the Fourier transform of the DAC's impulse response function $h_1(t)$.

For the second DAC, which generates the alternate samples, the sampling clock is supplied with a delay of T_s. Therefore, its Fourier transform $Y_2(\omega)$ would have identical $X(\omega)$ but it has its own impulse response with 180 degree phase rotation in every zone (that is, the frequency range between adjacent Nyquist frequencies). In this way, image signals created in the second zone are, ideally, cancelled, where

$$\begin{aligned} Y_2(\omega) &= \sum_{n=-\infty}^{\infty} X\left(\omega - \frac{(n-1)\pi}{T_s}\right) H_2(\omega) e^{j(n-1)\pi} \\ &= \sum_{n=-\infty}^{\infty} X\left(\omega - \frac{(n-1)\pi}{T_s}\right) [H_1(\omega) H_{imb}(\omega)] e^{j(n-1)\pi}. \end{aligned} \quad (3)$$

The Nyquist zone is defined as the frequency range between neighboring integer-multiple frequencies of the Nyquist frequency. Thus, because the sampling rate of the individual DAC is 10 Gsps, we define the first zone as the frequency range between 0 to 5 GHz (with zone number $n = 1$).

At the output of each path, signals are summed, to generate $Y(\omega)$, in which the overall frequency response is expressed by the common response ($H_1(\omega)$) and the imbalance response ($H_{imb}(\omega)$):

$$\begin{aligned} Y(\omega) &= Y_1(\omega) + Y_2(\omega) \\ &= \sum_{n=-\infty}^{\infty} X\left(\omega - \frac{(n-1)\pi}{T_s}\right) [H_1(\omega) \pm H_2(\omega)] \begin{pmatrix} +: n \text{ odd} \\ -: n \text{ even} \end{pmatrix} \\ &= \sum_{n=-\infty}^{\infty} X\left(\omega - \frac{(n-1)\pi}{T_s}\right) H_1(\omega) [1 \pm H_{imb}(\omega)]. \end{aligned} \quad (4)$$

In (4), images in zones with a negative sign (where n is even) are cancelled out, resulting in the ideal Fourier transform of the original $x(t)$ sampled at a period of T_s.

In the implementation of the overall system, which is shown in Fig. 1, there are non-idealities such as timing errors and gain mismatches between time-interleaved paths caused by imperfect manufacturing processes. Even a small amount of mismatch adversely affects image cancellation and the signal-to-noise ratio.

III. Identification of Nonidealities

To identify and correct DAC nonidealities, we conducted measurements with a commercially available AWG with time-interleaved DACs. The test signal was generated with a sampling rate of 20 Gsps at a center frequency of 4 GHz, representing a 64-QAM modulated signal. The signal had a data rate of 1 Gsps, with an occupied bandwidth of approximately 1.25 GHz. The signal from the AWG was captured with a high-speed sampling oscilloscope and the data were post-processed with an accurate time-base distortion correction algorithm [6],[7].

For the first step of the procedure, the frequency response of each path was identified by separately uploading the time-interleaved waveforms one at a time, while the other DAC was given all zeros. The two measured signals, when combined, represent the composite response of the ideal $X(\omega)$ and the impulse responses of the individual paths, $H_1(\omega)$ and $H_2(\omega)$:

$$Y(\omega)_{x_2=0} = Y_1(\omega) + N_o = \sum_{n=-\infty}^{\infty} X\left(\omega - \frac{(n-1)\pi}{T_s}\right) H_1(\omega) + N_o \quad (5)$$

and

$$\begin{aligned} Y(\omega)_{x_1=0} &= Y_2(\omega) + N_o \\ &= \sum_{n=-\infty}^{\infty} X\left(\omega - \frac{(n-1)\pi}{T_s}\right) H_2(\omega) e^{j(n-1)\pi} + N_o \end{aligned}, \quad (6)$$

where N_o is the total random noise across the bandwidth B from various noise sources such as thermal noise and quantization noise [8].

The n^{th} zone frequency response of the k^{th} DAC path within the signal bandwidth B may be given as follows:

$$H_k(\omega)_{n^{th}-zone} = \frac{Y_k(\omega)_{n^{th}-zone}}{X\left(\omega - \frac{(n-1)\pi}{T_s}\right)}, \quad |\omega - \omega_c| \le B/2. \quad (7)$$

Figure 2 shows the first- and second-zone spectral response of the signal from the AWG with a combined sampling frequency of 20 Gsps (blue, solid line), measured after passing through a low-pass filter with a cut-off frequency of 7 GHz. In the figure, the residual image signal in the second zone (5 to 10 GHz) is quite significant because of the imbalance, despite the AWG's built-in calibration process. By taking the difference of (5) and (6), the in-band (n = 1) and image-band (n = 2) residual error with noise can be observed and is shown in Figure 2 as well (red, dotted line). In this particular case, we assume that the spectral components from DAC #1 have sufficient signal-to-noise ratio within the bandwidth of the signal, and, thus, the responses in the first two zones may be identified.

To obtain the imbalance information in the frequency domain, the spectral components of DAC #1 and DAC #2 are compared within a bandwidth of B for the first two zones, where, again, a high signal-to-noise ratio is assumed:

$$H_{imb}(\omega)_{n^{th}-zone} = \frac{H_2(\omega - n\omega_s)}{H_1(\omega - n\omega_s)}, \quad |\omega - n\omega_s - \omega_c| \le B/2. \quad (8)$$

Figure 3(a) shows the identified magnitude response $|H_{imb}(\omega)|$ over the signal bandwidth within the first two zones.

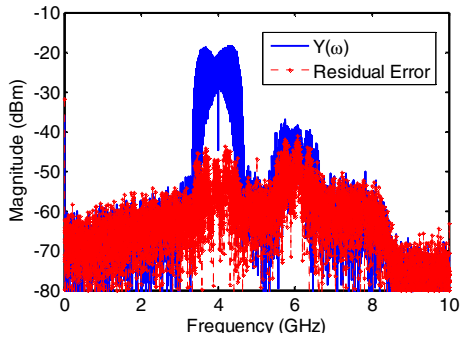

Fig. 2. Measured response (solid line) of a 1 Gsps 64-QAM signal generated with an AWG sampling frequency of 20 Gsps and the residual error due to DAC imbalance (dotted line).

This residual error corresponds to the cancellation path that is not exactly 180º over the band of interest. Additionally, Figure 3(b) shows the common frequency response $|H_1(\omega)|$ of the overall system over the same frequency range, which can be identified by (8). We see that the system obviously has highly frequency-dependent non-idealities.

To correct these non-idealities, a pre-filter that compensates for the in-band imbalance in the first zone (below the Nyquist frequency of DAC #2) is applied to the DAC #2 waveform. This filter is placed at the output of DAC #2, and has the inverse response of (8) over the desired bandwidth. In a similar manner, a pre-filter that has the inverse response of $H_1(\omega)$, the common frequency response from (7), is applied to the sum of the DAC outputs. Figure 4 shows the final block diagram. This figure shows the pre-filtering blocks for the common- and imbalance- response corrections.

The correction performance was evaluated with the EVM metric, which was 1.8 %, compared to 8.9 % without the correction. Furthermore, the value could be improved to a nominal value of 0.7 % when the correction method was incorporated with an iterative pre-distortion technique to remove additional excitation-dependent, nonlinear distortion [1].

An uncertainty analysis based on the NIST Microwave Uncertainty Framework [9, 10] included more than 640 error mechanisms. This analysis included a wide array of parameters from the pin depth of the calibration standards, to effects of cable bend, to optical parameters for the electro-optic sampling system used to calibrate the sampling oscilloscope. This analysis found an overall mean error in the EVM of approximately 1.0 % ± 0.3%, with measurement repeatability being the largest source of error.

IV. Conclusion

We presented a correction method for use in generating multi-gigabit-per-second signals with AWGs that include time-interleaved DACs. With this method, we first identify and pre-filter the imbalance between DAC paths. We then identify and pre-filter the linear response of the system. With this proposed method, we improved the EVM from 8.9 % to 1.8 % for a 1 Gsps, 64-QAM modulated signal with a 4 GHz carrier frequency. This could be further improved to ~1.0 % by iteratively correcting complex frequency coefficients to compensate for both linear and nonlinear distortion.

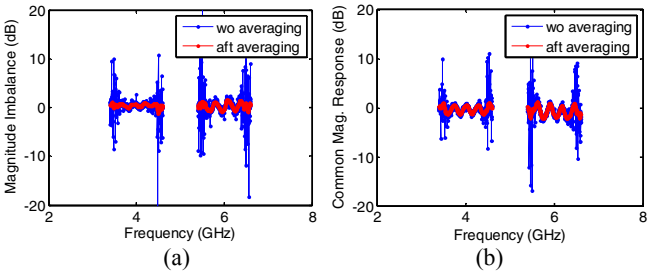

Fig. 3. Identified magnitude responses over the signal bandwidth within the first two zones: (a) Imbalance response (b) Common response.

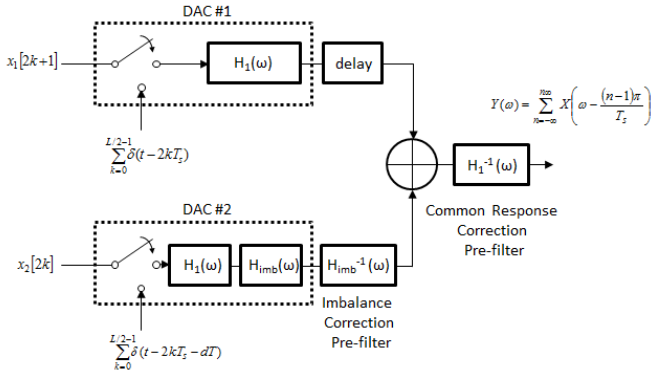

Fig. 4. Correction of frequency-dependent non-idealities by pre-filters to correct the imbalance- and common-frequency responses.

V. Acknowledgment

The authors acknowledge NIST researchers Dylan Williams, Paul Hale, Chih-Ming Wang, and Jeff Jargon for their support of this work in the context of the NIST project "Traceability to Enable Multi-GigaBit-per-Second Mobile Wireless."

References

[1] K. A. Remley, P. D. Hale, D. F. Williams, and C.-M. Wang, "A precision millimeter-wave modulated-signal source," *IEEE Int. Microwave Symp. Dig.,* Seattle, WA, June 2-7, 2013, Paper TH2D-3.

[2] Tomorrow Works (2013, May 13), "Samsung Announces World's First 5G mmWave Mobile Technology" *Samsung Tomorrow* [Online]. Available: http://global.samsungtomorrow.com/?p=24093

[3] *Application Note: 76W-29216-0, Understanding AWG70000A Series Frequency Response and DAC Performance*, Tektronix, Beaverton, OR, 2013.

[4] W. C. Black and D. A. Hodges, "Time interleaved converter arrays," *IEEE J. Solid-State Circuits*, vol. SC-15, no. 6, pp. 1022-1029, Dec. 1980.
[5] C. Krall, C. Vogel, and K. Witrisal,"Time-interleaved digital-to-analog converters for UWB signal generation," *IEEE Int. Conf. Ultra-Wideband,* Singapore, pp. 24-26, Sept. 2007.
[6] C.-M. Wang, P.D. Hale, J.A. Jargon, D.F. Williams, and K.A. Remley, "Sequential estimation of timebase corrections for an arbitrarily long waveform," *IEEE Trans. Inst. and Meas.*, vol. 61, no. 10, pp. 2689-2694, October, 2012.
[7] D. F. Williams, P. D. Hale, K. A. Remley, "The sampling oscilloscope as a microwave instrument," *IEEE Microwave Mag.*, vol. 8, issue 4, pp.59-68, April, 2007.
[8] J. Mitola III, *Software Ratio Architecture*, John Wiley & Sons, Inc., New York, NY, 2000.
[9] NIST Microwave Uncertainty Framework, Beta Version, D. F. Williams, http://www.nist.gov/pml/electromagnetics/related-software.cfm , 2012.
[10] J. A. Jargon, D. F. Williams, T. M. Wallis, D. X. LeGolvan, and P. D. Hale, "Establishing Traceability of an Electronic Calibration Unit Using the NIST Microwave Uncertainty Framework," *79th ARFTG Conf. Dig.*, pp. 32-36, Montreal, Canada, Jun. 2012.